Quantum oscillations in the linear chain of coupled orbits: the organic metal with two cation layers θ-$(ET)_4CoBr_4(C_6H_4Cl_2)$

A. Audouard[1], J.-Y. Fortin[2], D. Vignolles[1], R. B. Lyubovskii[3], L. Drigo[1], F. Duc[1], G. V. Shilov[3] G. Ballon[1], E. I. Zhilyaeva[3], R. N. Lyubovskaya[3] and E. Canadell[4]

[1] *Laboratoire National des Champs Magnétiques Intenses (UPR 3228 CNRS, INSA, UJF, UPS) 143 avenue de Rangueil, F-31400 Toulouse, France.*
[2] *Institut Jean Lamour, Département de Physique de la Matière et des Matériaux, Groupe de Physique Statistique, CNRS-Nancy-Université BP 70239 F-54506 Vandoeuvre les Nancy Cédex, France.*
[3] *Institute of Problems of Chemical Physics, RAS, 142432 Chernogolovka, MD, Russia.*
[4] *Institut de Ciència de Materials de Barcelona, CSIC, Campus de la UAB, 08193, Bellaterra, Spain.*

PACS 71.18.+y – Fermi surface: calculations and measurements; effective mass, g factor.
PACS 71.20.Rv – Polymers and organic compounds.
PACS 72.15.Gd – Galvanomagnetic and other magnetotransport effects.

Abstract – Analytical formulae for de Haas-van Alphen (dHvA) oscillations in linear chain of coupled two-dimensional (2D) orbits (Pippard's model) are derived systematically taking into account the chemical potential oscillations in magnetic field. Although corrective terms are observed, basic (α) and magnetic breakdown-induced (β and 2β - α) orbits can be accounted for by the Lifshits-Kosevich (LK) and Falicov-Stachowiak semiclassical models in the explored field and temperature ranges. In contrast, the 'forbidden orbit' β - α amplitude is described by a non-LK equation involving a product of two classical orbit amplitudes. Furthermore, strongly non-monotonic field and temperature dependence may be observed for the second harmonics of basic frequencies such as 2α and the magnetic breakdown orbit $\beta + \alpha$, depending on the value of the spin damping factors. These features are in agreement with the dHvA oscillation spectra of the strongly 2D organic metal θ-$(ET)_4CoBr_4(C_6H_4Cl_2)$.

Introduction. – Quasi-two-dimensional (q-2D) multiband organic compounds $(ET)_2X$ (where ET stands for the bis-ethylenedithio-tetrathiafulvalene molecule and X is a monovalent anion) exhibit very rich phase diagrams with ground states ranging from antiferromagnetic insulator to Fermi liquid. In particular, superconducting and magnetic ordered phases are observed close to each other which is reminiscent of cuprates and iron-based superconductors (for a recent review, see [1] and references therein). These compounds share the same Fermi surface (FS) topology which is an illustration of the linear chain of coupled orbits introduced by Pippard in the early sixties [2]. Such FS is liable to give rise to a network of orbits coupled by magnetic breakdown (MB) in large magnetic fields. Quantum oscillations in such systems have been extensively studied during the two last decades (for a review, see *e.g.* [3] and references therein). The main feature of the oscillation spectra of these com-

pounds is the presence of frequency combinations that are forbidden in the framework of the semiclassical model of Falicov-Stachowiak [4]. Theoretical studies have demonstrated that these Fourier components result from both the formation of Landau bands due to coherent MB, instead of discrete levels, and the oscillation of the chemical potential enabled by the 2D character of the FS. However, easy to handle analytic tools necessary to quantitatively account for the data are still lacking. As a matter of fact, comprehensive theoretical calculations taking into account coherent MB and oscillation of the chemical potential have been reported in Ref. [5] and implemented in de Haas-van Alphen (dHvA) data of the above mentioned compound. Nevertheless, as pointed out in Ref. [5], equations are complex and data could be analyzed only numerically.

The aim of this paper is therefore to provide analytical formulae accounting for quantum oscillation spectra of these systems. In the first step, analytical calculation of the Fourier amplitude of the various dHvA oscillations predicted for the FS illustrating the Pippard's model is reported. In the second step, the FS of the recently synthesized strongly 2D charge transfer salt θ-$(ET)_4CoBr_4(C_6H_4Cl_2)$ [6] is presented and, in the third step, analysis of the observed field- and temperature-dependent quantum oscillation spectra are reported. An excellent agreement with the calculations is obtained.

Experimental. – The studied crystals were synthesized by electrocrystallization technique as reported in Ref. [6]. They are elongated hexagonal platelets with approximate dimensions $1.5 \times 0.5 \times 0.04$ mm^3. X-ray diffraction data were collected both at room temperature in Chernogolovka with a KM-4 single-crystal diffractometer (Kuma Diffraction) and at 100 K with an Xcalibur diffractometer (Oxford Diffraction) at the Laboratoire de Chimie de Coordination in Toulouse. Tight-binding band structure calculations were based upon the effective one-electron Hamiltonian of the extended Hückel method [7], as reported *e.g.* in Ref. [8]. Magnetic torque and magnetoresistance were measured in pulsed magnetic fields of up to 55 T with a pulse decay duration of 0.32 s. Magnetic torque measurements were performed with a commercial piezoresistive microcantilever [9] in the temperature range from 1.4 K to 4.2 K. The size of the sample studied was approximately $0.12 \times 0.1 \times 0.04$ mm^3. Variations of the cantilever piezoresistance was measured with a Wheatstone bridge with an *ac* excitation at a frequency of 63 kHz. The angle between the normal to the conducting plane and the magnetic field direction was $\theta = 7°$. Magnetoresistance was measured thanks to a contactless radio frequency measurement technique based on tunnel diode oscillator as reported in Ref. [10]. A pair of counter-wound coils made with copper wire of 50 μm in diameter was used. As pointed out in [11], in the case where the interlayer resistivity is much larger than the in-plane resistivity, the contribution of the former parameter to the measured signal is negligible. The time evolution of the oscillator frequency during the field pulse is deduced from successive short-term fast Fourier transforms of the raw signal. In contrast, analysis of the oscillatory magnetoresistance and magnetic torque is based on discrete Fourier transforms of the field-dependent data, calculated with a Blackman window after removal of a non-oscillating background. Zero-field interlayer and in-plane 4-point resistance was measured with 1 μA *ac* current at 77 Hz. Electrical contacts were made using annealed platinum wires of 20 μm in diameter glued with graphite paste.

Calculation of de Haas-van Alphen amplitudes. – We consider a two-band system with band extrema $\Delta_{0(1)}$ (see Fig. 1(c)) and effective masses $m_{0(1)}$. In the low temperature limit, the grand potential Ω of a two-dimensional slab with area $\mathcal{A}$ is given by a series of harmonics p of classical frequencies F_η:

$$\frac{\Phi_0}{\mathcal{A}}\frac{u_0}{k_B}\Omega(T,\mu) = -\frac{m_0}{2}(\mu-\Delta_0)^2 - \frac{m_1}{2}(\mu-\Delta_1)^2 + \frac{(B\cos\theta)^2}{2}\sum_{p\geq 1}\sum_{\eta}\frac{C_\eta}{\pi^2 p^2 m_\eta}R_{\eta,p}(T,B)\cos(2\pi p\frac{F_\eta}{B\cos\theta}+p\varphi_\eta), \quad (1)$$

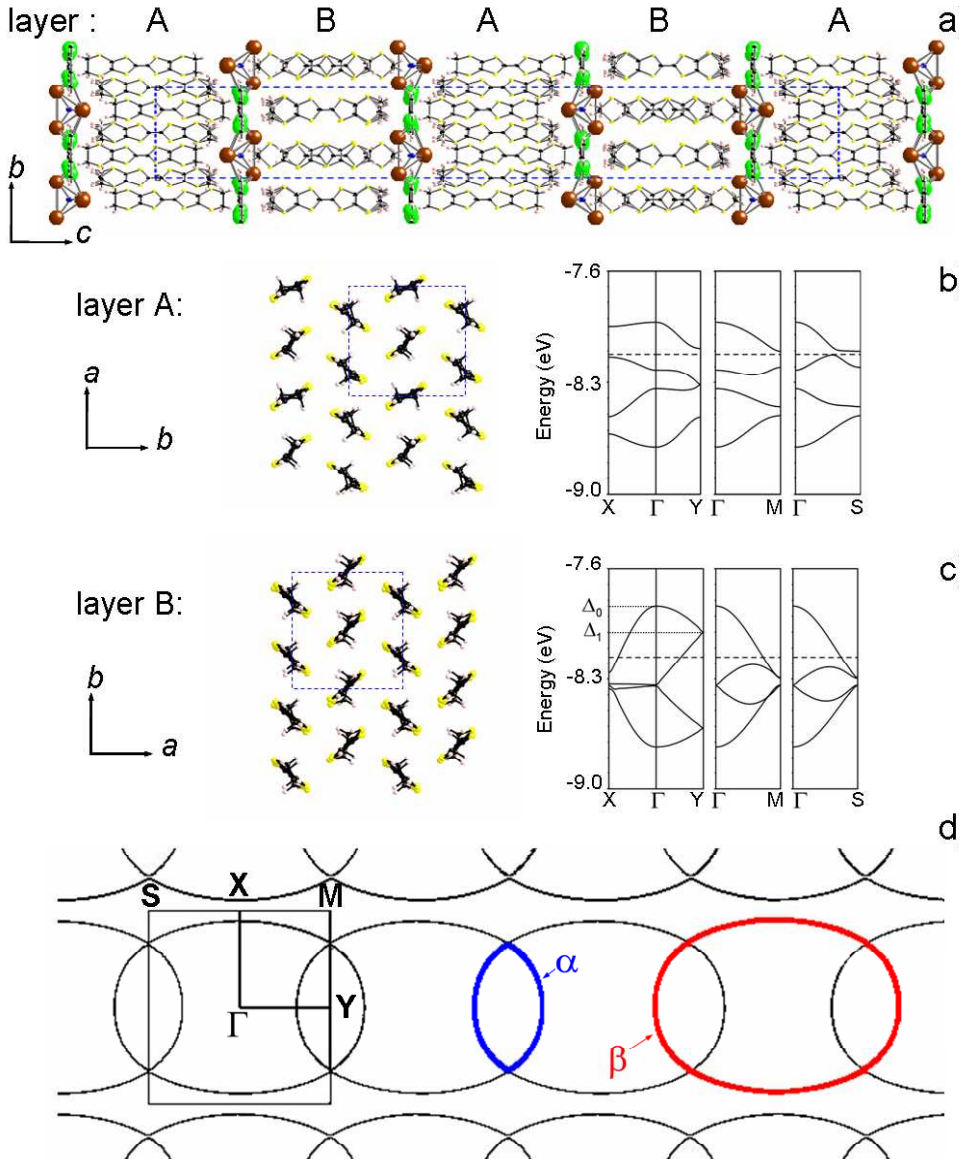

Fig. 1: (Colour on-line) (a) Crystal structure of θ-$(ET)_4CoBr_4(C_6H_4Cl_2)$ projected along the a direction. Two different cation layers labeled A and B, respectively, are evidenced. Atomic arrangement of the ET molecules plane and band structure calculations relevant to (b) insulating layer A and (c) metallic layer B. (d) Fermi surface relevant to layer B. Dashed line marks the top of the highest occupied band and the Fermi level in (b) and (c), respectively. Labels Δ_0 and Δ_1 stand for the band extrema. Γ, X, Y, M and S refer to (0, 0), (a^*/2, 0), (0, b^*/2), (a^*/2, b^*/2) and (a^*/2, -b^*/2), respectively.

where $\Phi_0 = h/e$ is the quantum flux and $u_0 = 2\pi^2 m_e k_B/e\hbar = 14.694$ T/K. Effective masses are expressed in m_e units and chemical potential μ in Tesla. The index η stands for all the possible classical orbits α, β, $\beta + \alpha$, 2β - α, *etc.*, excluding their harmonics, with frequencies $F_\eta = m_\eta(\mu$ - $\Delta_\eta)$ and effective masses m_η. Frequencies F_η depend on the chemical potential μ since they represent a filling factor corresponding to classical orbits. Coefficient C_η is the symmetry factor of the orbit η. For example, $C_\alpha = C_\beta = C_{2\beta-\alpha} = 1$ and $C_{\beta+\alpha} = 2$. φ_η is the phase of the orbit η, *i.e.* $\pi/2$ times the number of extrema of the

orbit in the k_x or k_y direction, for example, $\varphi_\alpha = \varphi_\beta = \varphi_{2\beta-\alpha} = \pi$ and $\varphi_{\beta+\alpha} = 2\pi$. These phases are important for determining the sign of amplitudes. In particular, we define two fundamental orbits with frequencies, $F_\alpha = m_1(\mu - \Delta_1)$ (*i.e.* $m_\alpha = m_1$) and $F_\beta = m_0(\mu - \Delta_0) + m_1(\mu - \Delta_1)$ which can be written as $F_\beta = m_\beta(\mu - \Delta_\beta)$ (see Fig. 1(d)). Therefore, $m_0 + m_1$ is identified to the effective mass m_β of the MB orbit β. The damping factors can be expressed as $R_{\eta,p}(T,B) = R^T_{\eta,p} R^D_{\eta,p} R^{MB}_{\eta,p} R^s_{\eta,p}$ where the thermal, Dingle, MB and spin damping factors are given by:

$$R^T_{\eta,p} = \frac{u_0 T p m_\eta}{B\cos\theta \sinh(\frac{u_0 T p m_\eta}{B\cos\theta})} \tag{2}$$

$$R^D_{\eta,p} = \exp(-\frac{u_0 T_D p m_\eta}{B\cos\theta}) \tag{3}$$

$$R^{MB}_{\eta,p} = (ip_0)^{n^t_\eta}(q_0)^{n^r_\eta} \tag{4}$$

$$R^s_{\eta,p} = \cos(\pi p \frac{g^* m_\eta}{2\cos\theta}), \tag{5}$$

respectively. T_D is the Dingle temperature ($T_D = \hbar/2\pi k_B\tau$ where τ is the relaxation time). Integers n^t_η and n^r_η are the (even) number of MB tunnelings and reflections, respectively, encountered by the quasiparticle along its closed trajectory. The MB tunneling and reflection probabilities are given by $p_0 = \exp(-B_0/2B)$ and $q_0^2 = 1 - p_0^2$, respectively, where B_0 is the MB field. g^* is the effective Landé factor[1]. The electron density per surface area n_e is given by $\mathrm{d}\Omega/\mathrm{d}\mu = -n_e$. In zero-field, Eq. 1 yields $n_e = (m_0 + m_1)\mu_0 - m_0\Delta_0 - m_1\Delta_1$. In presence of a magnetic field, μ satisfies the following implicit equation:

$$\mu = \mu_0 - \frac{B\cos\theta}{m_\beta} \sum_{p\geq 1}\sum_\eta \frac{1}{\pi p} C_\eta R_{\eta,p}(T,B) \sin(2\pi p \frac{F_\eta}{B\cos\theta} + p\varphi_\eta) \tag{6}$$

The oscillating part of the magnetization can be computed systematically by inserting Eq. 6 in Eq. 1 and deriving the resulting expression with respect to the magnetic field. Direct numerical resolution of this implicit equation could be done. Besides, a more user-friendly controlled expansion in term of damping factors $R_{\eta,p}$ can be derived systematically at any possible order. Keeping successive terms in powers of $R_{\eta,p}$ up to the second order, yields analytically the following expression for the oscillating part of the magnetization:

$$\begin{aligned} m_{osc} &= -\sum_\eta \sum_{p\geq 1} \frac{F_\eta C_\eta}{\pi p m_\eta} R_{\eta,p}(T,B) \sin\left(2\pi p \frac{F_\eta}{B\cos\theta} + p\varphi_\eta\right) \\ &+ \sum_{\eta,\eta'} \sum_{p,p'\geq 1} \frac{F_\eta C_\eta C_{\eta'}}{\pi p' m_\beta} R_{\eta,p}(T,B) R_{\eta',p'}(T,B) \left[\sin\left(2\pi \frac{pF_\eta + p'F_{\eta'}}{B\cos\theta} + p\varphi_\eta + p'\varphi_{\eta'}\right)\right. \\ &- \left.\sin\left(2\pi \frac{pF_\eta - p'F_{\eta'}}{B\cos\theta} + p\varphi_\eta - p'\varphi_{\eta'}\right)\right] + \cdots \end{aligned} \tag{7}$$

where frequencies F_η are evaluated at $\mu = \mu_0$, namely, $F_\eta = m_\eta(\mu_0 - \Delta_\eta)$. Eq. 7 can be written as a sum of periodic functions with frequencies F_i and Fourier amplitudes A_i where the index i stands for either classical orbits η or 'forbidden' orbits such as β - α. Relevant examples for experimental analysis are given below:

[1] FS warping can be accounted for by the additional damping factor $\mathrm{J}_0(4\pi p m_\eta \tau_\perp/e\hbar B)$, where $\tau_\perp$ is the interlayer transfer integral [12]. In most q-2D organic metals, this factor is close to 1.

$$A_\alpha = \frac{F_\alpha}{\pi m_\alpha} R_{\alpha,1} + \frac{F_\alpha}{2\pi m_\beta} R_{\alpha,1} R_{\alpha,2} + \frac{F_\alpha}{6\pi m_\beta} R_{\alpha,2} R_{\alpha,3} + \frac{2F_\alpha}{\pi m_\beta} R_{\beta,1} R_{\alpha+\beta,1}, \quad (8)$$

$$A_{2\alpha} = -\frac{F_\alpha}{2\pi m_\alpha} R_{\alpha,2} + \frac{F_\alpha}{\pi m_\beta} R_{\alpha,1}^2 - \frac{2F_\alpha}{3\pi m_\beta} R_{\alpha,1} R_{\alpha,3}, \quad (9)$$

$$A_\beta = \frac{F_\beta}{\pi m_\beta} R_{\beta,1} + \frac{F_\beta}{2\pi m_\beta} R_{\beta,1} R_{\beta,2} + \frac{F_\beta}{6\pi m_\beta} R_{\beta,2} R_{\beta,3} + \frac{2F_\beta}{\pi m_\beta} R_{\beta,1} R_{\alpha+\beta,1}, \quad (10)$$

$$A_{2\beta} = -\frac{F_\beta}{2\pi m_\beta} R_{\beta,2} + \frac{F_\beta}{\pi m_\beta} R_{\beta,1}^2 - \frac{2F_\beta}{3\pi m_\beta} R_{\beta,1} R_{\beta,3}, \quad (11)$$

$$A_{\beta-\alpha} = -\frac{F_{\beta-\alpha}}{\pi m_\beta} R_{\alpha,1} R_{\beta,1} - \frac{F_{\beta-\alpha}}{\pi m_\beta} R_{\alpha,2} R_{\alpha+\beta,1} - \frac{F_{\beta-\alpha}}{\pi m_\beta} R_{\beta,2} R_{\alpha+\beta,1}, \quad (12)$$

$$A_{\beta+\alpha} = -\frac{2F_{\beta+\alpha}}{\pi m_{\beta+\alpha}} R_{\beta+\alpha,1} + \frac{F_{\beta+\alpha}}{\pi m_\beta} R_{\alpha,1} R_{\beta,1}, \quad (13)$$

$$A_{2\beta-\alpha} = \frac{F_{2\beta-\alpha}}{\pi m_{2\beta-\alpha}} R_{2\beta-\alpha,1} + \frac{F_{2\beta-\alpha}}{2\pi m_\beta} R_{\alpha,1} R_{\beta,2} + \frac{F_{2\beta-\alpha}}{6\pi m_\beta} R_{\alpha,3} R_{\alpha+\beta,2}. \quad (14)$$

In the framework of the LK model, the amplitude of a Fourier component linked to a basic orbit involves only one damping factor (*e.g.* $A_\alpha \propto R_\alpha$). This is also the case for a MB orbit, the effective mass of which is given by the Falicov-Stachowiak model (*e.g.* $m_{2\beta-\alpha} = 2m_\beta$ - m_α) [4]. According to this statement, the leading term of Eqs. 8 and 10 which accounts for the α and β components, respectively, reproduces the LK equation. Furthermore, deviations from the LK behaviour due to the high order terms involving products of damping factors are only significant in the low temperature and high field ranges. This statement also stands for 2β-α since $R_{2\beta-\alpha}$ is significantly higher than the product $R_{\alpha,1}R_{\beta,2}$ (see Eq. 14). As a consequence, the Falicov-Stachowiak model should apply for this component as well. In contrast, algebraic sum of damping terms in Eqs. 9 and 13, where minus signs accounts for π dephasings, may cancel at field and temperature values dependent on the effective masses, Dingle temperature, MB field, *etc.* as displayed in Fig. 2 relevant to 2α. This point has already been reported for the second harmonic of the basic orbits both for compensated [13] and un-compensated [14] metals. In that respect, since algebraic sums are involved, care must be taken of the spin damping factor sign[2]. Indeed, the value of the spin damping factor, which is changed through the value of g^* in Fig. 2, can have a drastic effect on the field and temperature dependence of the amplitude in this case. Finally, the Fourier amplitude of the 'forbidden orbit' β - α is accounted for by Eq. 12. Although a non-LK behaviour is evidenced, a monotonic field and temperature dependence is expected owing to the negligibly small value of the high order terms. The consistency of Eqs. 8 to 14 with experimental data is examined in the next section.

Results and discussion. – Even though the organic metal θ-$(ET)_4CoBr_4(C_6H_4Cl_2)$ undergoes a phase transition at 343 K [6], no additional phase transition is revealed by X-ray diffraction below room temperature, at which crystals are synthesized, down to 100 K. As displayed in Fig. 1, the central feature of the crystalline structure at room temperature is that the unit cell has two different donors planes labeled A and B. According to band structure calculations, layer A is insulating while layer B is metallic. FS of layer B is composed of one closed tube centered at Y with an area of 18 % of the first Brillouin zone (FBZ) area (yielding α orbit in magnetic field) and two q-1D sheets with rather small gap in between. Therefore, it is expected that the MB orbit β, which corresponds to the hole tube centered at Γ with an area equal to that of the FBZ is observed in moderate fields, giving rise to the textbook

[2]Since the LK equation involves a single damping term, the absolute value of the spin damping factor is considered in the case where data are analyzed on this basis. However, π dephasing is observed on either side of spin-zero angles as reported in [15].

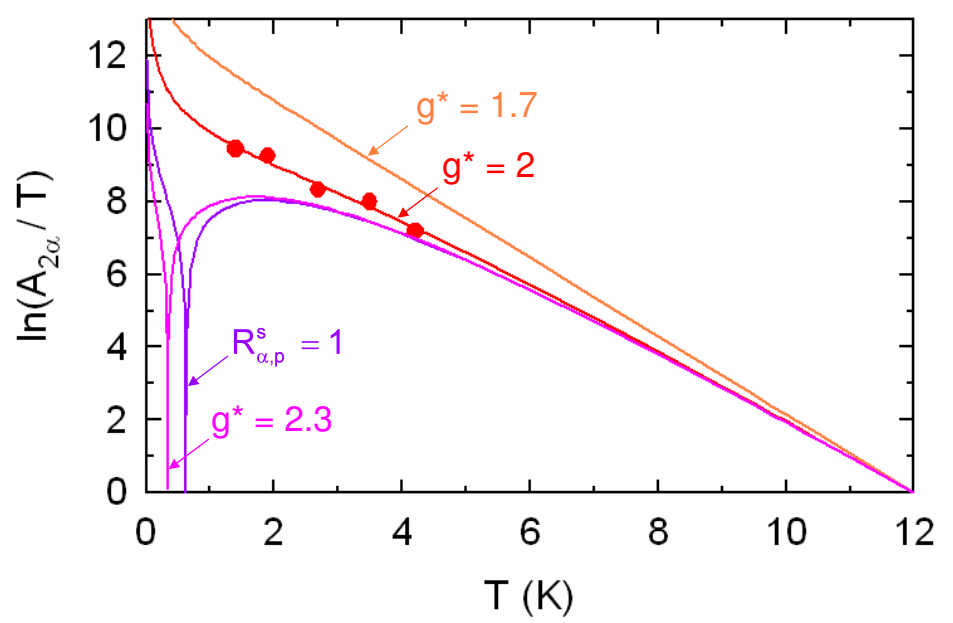

Fig. 2: (Colour on-line) Temperature dependence (mass plot) of the amplitude of the component 2α. Symbols are data deduced from torque measurements of Fig. 4(a) at 48.3 T. Solid lines are deduced from Eq. 9 with $m_\alpha = 1.81$, $m_\beta = 3.52$, $T_D = 0.79$ K and $B_0 = 35$ T. Spin damping factor (see Eq. 5) is either neglected ($R^s_p = 1$, p = 1 to 3) or accounted for by various g^* values. All the data are normalized to their values at 12 K.

linear chain of coupled orbits. In addition, since layers A are insulating, conducting planes are strongly separated from each other which suggests a strongly 2D behaviour. In line with this statement, the room temperature resistivity anisotropy ρ(interlayer)/ρ (in plane) is as large as 10^4 [6]. Furthermore, according to the data in Fig. 3, this anisotropy further increases up to ρ(interlayer)/ρ(in plane) = 10^6 as the temperature decreases down to liquid helium temperatures.

Magnetic torque (dHvA oscillations) and tunnel diode oscillator [Shubnikov-de Haas (SdH) oscillations] data are displayed in Fig. 4. Besides Fourier components linked to the closed orbit α and to the MB orbit β, few frequency combinations typical of the FS displayed in Fig. 1 are observed in the high field range of the torque spectra. In contrast, numerous combinations are observed in SdH spectra. As an example, the Fourier component 2β - 3α is clearly detected in Fig. 4(b). This frequency, which to our knowledge is observed for the first time, could correspond to a quantum interferometer path. However, its amplitude is unexpectedly large. The frequencies linked to the β and α orbits are $F_\beta(\theta = 0) = 4600 \pm 10$ T, in agreement with the FBZ area at 100 K, and $F_\alpha(\theta = 0) = 944 \pm 4$ T, respectively. The latter value yields a cross section area of 20.6 % of the FBZ area, in satisfactory agreement with the band structure calculations of Fig. 1. Field- and temperature-dependent Fourier amplitudes can be studied at the light of the results given in the preceding section, keeping in mind that dHvA amplitudes A_η are related to torque oscillation amplitudes A^τ_η as $A_\eta \propto A^\tau_\eta / B\tan(\theta)$. Effective masses, derived from Eq. 8 at various magnetic field values are field-independent: $m(\alpha) = 1.81 \pm 0.05$, $m(\beta) = 3.52 \pm 0.19$ (see Fig. 5(a)). In agreement with results of Ref. [16], $m(\beta)$ is twice $m(\alpha)$ within the error bars. At odds with torque results, effective masses deduced from SdH data, in particular those relevant to the β component, definitely increase as the magnetic field increases. This behaviour indicates that the above calculations, relevant to dHvA oscillations, cannot account for the SdH data at high field.

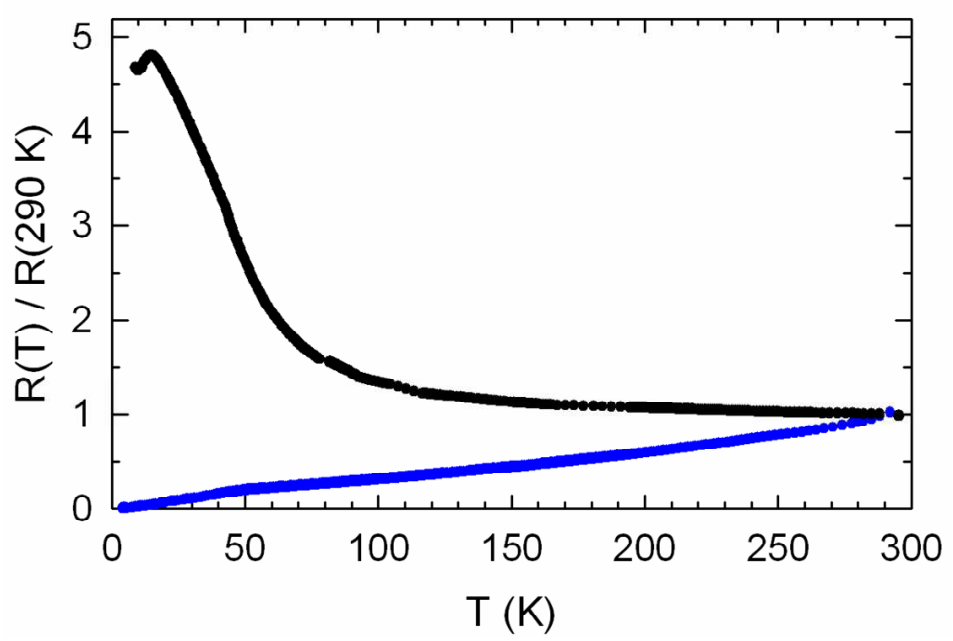

Fig. 3: (Colour on-line) Temperature dependence of zero-field in-plane (blue lower curve) and interlayer (black upper curve) resistance normalized to the values at 290 K.

Focusing on dHvA oscillations, Dingle plots of α and β can be obtained plotting $A^{\tau}_{\eta}/BR^{T}_{\eta,1}$ where $R^{T}_{\eta,1}$ is given by Eq. 2, assuming the LK formalism accounts for the data, i.e. the high orders terms of Eq. 8 can be neglected. As reported in Fig. 5, all the data relevant to the α and β components lies, respectively, on the same curve within the experimental scattering which suggests that the above assumption holds. Dingle temperature and MB

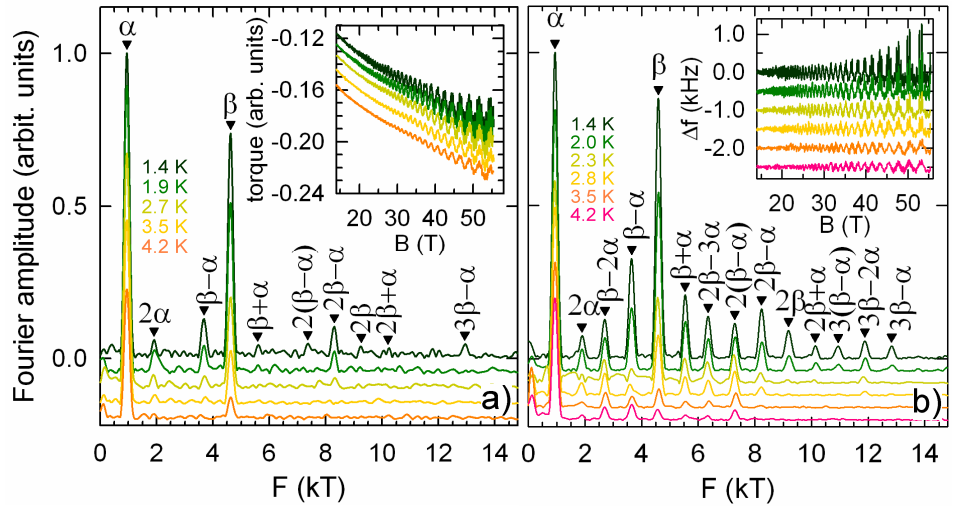

Fig. 4: (Colour on-line) Fourier analysis in the field range 35-55.3 T of (a) the magnetic torque data (dHvA oscillations) and (b) the tunnel diode oscillator data (SdH oscillations) reported in the respective insets. Solid triangles are marks calculated with $F_{\alpha}(\theta = 0) = 0.944$ kT and $F_{\beta}(\theta = 0) = 4.60$ kT. Data have been shifted down from each other by a constant amount.

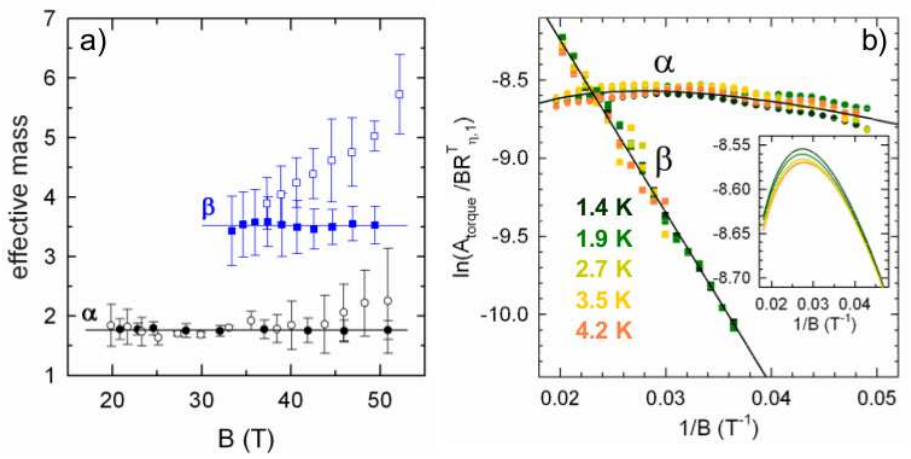

Fig. 5: (Colour on-line) (a) Effective masses vs. magnetic field for the α (circles) and β (squares) oscillations deduced from best fits of Eq. 8 to the torque (solid symbols) and tunnel diode oscillator (open symbols) data. Horizontal lines stand for the mean values of the effective masses deduced from torque data ($m_\alpha = 1.81$, $m_\beta = 3.52$). (b) Dingle plot of the α and β torque oscillations. $R^T_{\eta,1}$, where $\eta = \alpha, \beta$, is calculated with m_α and m_β deduced from (a). Solid lines are best fits of Eq. 8 and 10 to the data relevant to α and β, respectively, obtained with $B_0 = 35$ T and $T_D = 0.79$ K (see Eqs. 2 to 4). Inset displays an enlarged view of the fits for α.

field can be derived for components which do not involve tunneling ($n^t_\eta = 0$ in Eq. 5). Although this is the case of α, a very broad maximum is observed in Fig. 5, leading to a very large uncertainty on the MB field. More specifically, B_0 values ranging from 0 to 70 T can account for the data, in which case T_D ranges from 1.4 to 0.5 K, respectively. Assuming the Dingle temperature linked to the α orbit is the same as that of β considerably reduces the uncertainty since the well defined slope $s_\beta = -(u_0 T_D m_\beta + 2B_0)$ of the Dingle plot for β yield an additional relationship between T_D and B_0. This assumption yields $B_0 = 35 \pm 5$ T and $T_D = 0.79 \pm 0.10$ K. With these values of effective masses, Dingle temperature and MB field, it is possible to check whether or not the high order terms of Eq. 8 can be neglected. Inset

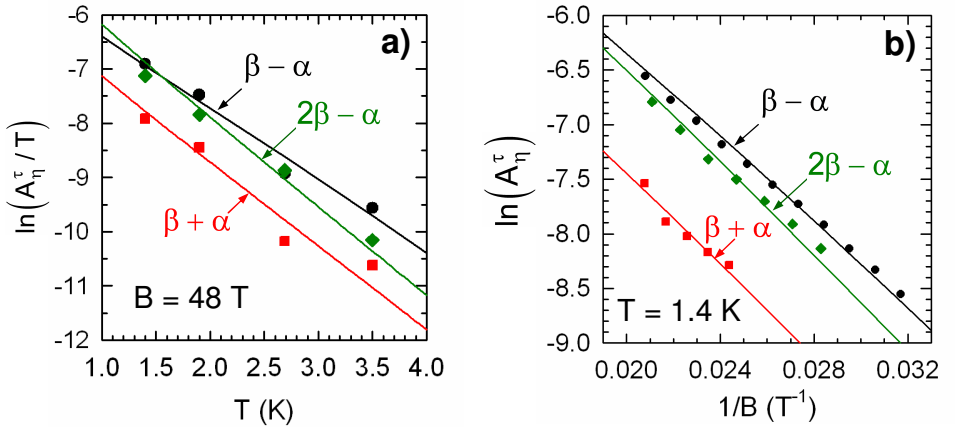

Fig. 6: (Colour on-line) (a) Mass plots and (b) Dingle plots of β - α (circles), β + α (squares) and 2β - α (diamonds). Solid lines are bests fits of Eqs. 12, 13 and 14, calculated with $m_\alpha = 1.81$, $m_\beta = 3.52$, $B_0 = 35$ T, $T_D = 0.79$ K and $g^* = 2$.

of Fig. 5(b) displays the field dependence of $A^{\tau}_{\alpha}/BR^{T}_{\alpha,1}$ calculated for the highest field range covered by the experiments, assuming further that $g^* = 2$[3]. Although the contribution of these factors rises as the field increases, it remains smaller than the experimental scattering for both α and β.

The field and temperature dependence of the Fourier amplitude relevant to frequency combinations is displayed in Fig. 6. Since their amplitude is much smaller than that of the orbits α and β, only mass plots at high field and Dingle analysis at the lowest explored temperature are considered. As already discussed for the second harmonics 2α (see Fig. 2), amplitudes are strongly dependent on the spin damping factors value. Solid lines in Fig. 6 are the best fits of Eqs. 12 to 14, obtained with the same values of m_α, m_β, B_0, T_D and g^* as above, with only a prefactor as a free parameter for each of the data: a very good agreement is obtained, in particular for the 'forbidden orbit' β - α. It can be remarked that the behaviour of both 2β - α and $\beta + \alpha$ are close to the predictions of the Falicov-Stachowiak model. Whereas this feature is mainly due to the small value of $R_{\alpha,1}R_{\beta,2}$ compared to $R_{2\beta-\alpha,1}$ in the former case, it can be attributed to the peculiar set of values of the spin damping factors ($R^s_{\alpha,1}R^s_{\beta,2}/R^s_{\beta+\alpha,1}$ = -0.22) in the latter case.

Summary and conclusion. – Analytical formulae for dHvA oscillations relevant to a class of FS illustrating the Pippard's model and observed in many q-2D organic conductors have been derived systematically taking into account the chemical potential oscillations in magnetic field (Eqs. 8 to 14). Although high orders terms are observed, basic (α) and MB-induced (β and 2β - α) orbits can be accounted for by the LK and Falicov-Stachowiak semiclassical models, at least at moderate fields and temperatures. In contrast, the 'forbidden orbit' β - α is accounted for by a non-LK equation, involving products of classical amplitudes relevant to α and β. Furthermore, strongly non-monotonic field and temperature dependence may be observed for the second harmonics of basic frequencies such as 2α and the MB orbit $\beta + \alpha$, depending on the value of the spin damping factor R^s_η.

These formulae are in agreement with the dHvA oscillation spectra of the strongly 2D organic metal θ-$(ET)_4CoBr_4(C_6H_4Cl_2)$, assuming $g^* = 2$. However, SdH oscillations spectra exhibit a tremendous number of Fourier components suggesting, besides quantum interference contributions, more severe deviations from the LK model that remains to be explained within a SdH theory including quantum interference contribution.

* * *

This work has been supported by EuroMagNET II under the EU contract number 228043, DGES-Spain (Projects FIS2009-12721-C04-03 and CSD2007-00041) and by the CNRS-RFBR cooperation under the PICS contract number 5708. We acknowledge the technical help of Laure Vendier at the X-ray facility of the LCC-Toulouse.

REFERENCES

[1] Haddad S.,Charfi-Kaddour S. and Pouget J.-P., *J. Phys.: Condens. Matter*, **23** (2011) 464205.
[2] Pippard A. B., *Proc. R. Soc. London*, **A 270** (1962) 1.
[3] Kartsovnik M. V., *Chem. Rev.*, **104** (2004) 5737.
[4] Shoenberg D., *Magnetic Oscillations in Metals*, edited by Cambridge University Press (Cambridge, England) 1984
[5] Gvozdikov V. M., Jansen A. G. M., Pesin D. A., Vagner I. D. and Wyder P., *Phys. Rev. B*, **70** (2004) 245114.
[6] Shilov G. V., Zhilyaeva E. I., Flakina A. M., Torunova S. A., Lyubovskii R. B., Aldoshin S. M., and Lyubovskaya R. N., *Cryst. Eng. Comm.*, **13** (2011) 1467.

[3]Effective Landé factor as low as $g^* = 1.5 \div 1.6$ are reported for the strongly correlated compound κ-$(ET)_2Cu(NCS)_2$ [5], nevertheless $g^* = 2$ is consistent with data of other ET salts [17, 18].

[7] Whangbo M.-H. and Hoffmann, R., *J. Am. Chem. Soc.*, **100** (1978) 6093.
[8] Audouard A., Duc F., Vignolles D., Lyubovskii R. B., Vendier L., Shilov G. V., Zhilyaeva E. I., Lyubovskaya R. N. and Canadell E., *Phys. Rev. B*, **84** (2011) 045101.
[9] Ohmichi E. and Osada T., *Rev. Sci. Inst.*, **73** (2002) 3022.
[10] Drigo L., Durantel F., Audouard A. and Ballon G., *Eur. Phys. J. Appl. Phys.*, **52** (2010) 10401.
[11] Ohmichi E., Komatsu E. and Osada, T., *Rev. Sci. Inst.*, **75** (2004) 2094.
[12] Champel T. and Mineev V. P., *Philos. Mag. B*, **81** (2001) 55.
[13] Fortin J.-Y. and Audouard A., *Phys. Rev. B*, **80** (2009) 214407.
[14] Fortin J.-Y., Perez E. and Audouard A., *Phys. Rev. B*, **71** (2005) 155101.
[15] Singleton J., *Rep. Prog. Phys.*, **60** (2000) 1111.
[16] Merino J. and McKenzie R. H., *Phys. Rev. B*, **62** (2000) 2416.
[17] Audouard A., Vignolles D., Haanappel E., Sheikin I., Lyubovskii R. B. and Lyubovskaya R. N., *Europhysics Letters*, **71** (2005) 783.
[18] Vignolles D., Audouard A., Laukhin V. N., Canadell E., Prokhorova T. G. and Yagubskii E. B., *Eur. Phys. J. B*, **71** (2009) 203.